Cadmium(II) complexes of *N*,*N*-diethyl-*N*′-benzoylthio(seleno)urea as single-source precursors for the preparation of CdS and CdSe nanoparticles

Jocelyn C. Bruce,[ab] Neerish Revaprasadu[b] and Klaus R. Koch*[a]

Received (in Durham, UK) 15th December 2006, Accepted 10th May 2007
First published as an Advance Article on the web 8th June 2007
DOI: 10.1039/b618254b

Cadmium complexes of *N*,*N*-diethyl-*N*′-benzoylthiourea and *N*,*N*-diethyl-*N*′-benzoylselenourea have been used as single-source precursors for the synthesis of HDA capped CdS and CdSe nanoparticles in a predominantly cubic phase, respectively. Both types of particles show quantum confinement effects and close to band edge luminescence. The particle morphology of CdS and CdSe nanoparticles obtained from the thermolysis of bis[*N*,*N*-diethyl-*N*′-(benzoylthioureato)]cadmium(II) and bis[*N*,*N*-diethyl-*N*′-(benzoylselenoureato)]cadmium(II) was found to be independent of the thermolysis temperature and monomer concentration in the ranges examined. The structure of the *N*,*N*-diethyl-*N*′-benzoylthiourea ligand was determined by single-crystal X-ray diffraction.

Introduction

The synthesis of highly crystalline, well coated, semiconducting nanocrystals of uniform shape and size has been the focus of considerable research interest in recent years.[1] These particles have a wide variety of promising applications due to their unique chemical and optical properties, particularly their size dependant emission.[2–6] The use of organometallic precursor compounds for the controlled synthesis of semiconducting quantum dots was pioneered by Bawendi and co-workers, however the noxious and hazardous nature of some of the starting compounds necessitates the need for safer synthetic routes.[7] To this end the use of single-source precursors has attracted significant attention and a variety of precursor complexes have been reported.[1,8–12] These include the cadmium complexes of alkyl substituted thioureas.[13]

As part of our long-standing interest in the coordination chemistry of *N*,*N*-dialkyl-*N*′-acyl(aroyl)thioureas, we here explore the synthesis of CdS and CdSe quantum dots from single-source precursor bis[*N*,*N*-diethyl-*N*′-(benzoylthioureato)]-cadmium(II)[14] and bis[*N*,*N*-diethyl-*N*′-(benzoylselenoureato)]-cadmium(II)[15] derived from ligands HL^1 and HL^2 in Fig. 1. These ligands readily form stable, bidentate O, S(Se) bound complexes with a wide variety of transition metal ions, following loss of the thioamidic proton or the selenoamidic proton.[16,17]

To our knowledge these complexes have not been used as single-source precursors before. Both ligands and metal complexes can be easily prepared in high yields from relatively inexpensive and only mildly hazardous starting materials, making them ideal for the potential large scale synthesis of CdS and CdSe nanoparticles.

[a] *Department of Chemistry and Polymer Science, University of Stellenbosch, P Bag X1, Matieland, 7602, South Africa. E-mail: krk@sun.ac.za; Fax: 021-8083342; Tel: 021 8083020*
[b] *Department of Chemistry, University of Zululand, Private Bag X1001, Kwadlangezwa, 3386, South Africa. E-mail: krk@sun.ac.za; Fax: 021-8083342; Tel: 021 8083020*

Experimental

Precursor synthesis

N,*N*-Diethyl-*N*′-benzoylthiourea (HL^1) and *N*,*N*-diethyl-*N*′-benzoylselenourea (HL^2) were synthesised and recrystallised according to literature methods.[18,19] The cadmium complexes of HL^1 and HL^2 were synthesised and recrystallised according to the method described in the literature.[15]

Chemicals

Sodium acetate, ethanol, toluene, methanol, hexadecylamine (HDA), tri-*n*-octylphosphine (TOP) and cadmium nitrate tetrahydrate were used as obtained from Aldrich. KSCN and KSeCN were dried in a vacuum oven immediately prior to use and acetone, diethyl amine and benzoyl chloride were distilled before use.

***N*,*N*-Diethyl-*N*′-benzoylthiourea.** Yield (87%); mp 99.8–100.7 °C. Found: C, 61.8; H, 5.9; N, 11.4. $C_{12}H_{16}N_2OS$ requires C, 61.1; H, 6.8; N, 11.9%. δ_H (400 MHz; $CDCl_3$): 1.28 (unres. t, 3H, H10/H12), 1.35 (unres. t, 3H, H10/H12), 3.59 (unres. q, 2H. H9/H11, 4.02 (unres. q, 2H, H9/H11), 7.45 (m, 2H, H3, H5), 7.56 (t, 1H, $^3J_{HH}$ = 7.5 and $^4J_{HH}$ = 1.3, H4), 7.82 (d, 2H. $^3J_{HH}$ = 7.5, H2, H6), 8.40 (br s, 1H, N–H). δ_C (100 MHz; $CDCl_3$): 11.4, 13.1 (C10, C12), 47.7, 47.9 (C9, C11), 127.8 (C3, C5), 128.8 (C2, C6), 132.6 (C1), 132.8 (C4), 163.7 (C7) 179.2 (C8).

***N*,*N*-Diethyl-*N*′-benzoylselenourea.** Yield (39.0%); mp 111.1–112.5 °C. Found: C, 51.0; H, 5.7; N, 9.9. $C_{12}H_{16}N_2OSe$ requires C, 50.9; H, 5.7; N, 9.9%. δ_H (600 MHz; $CDCl_3$): 1.30 (t, 3H, $^3J_{HH}$ = 7.2, H10/H12), 1.40 (t, 3H, $^3J_{HH}$ = 7.0, H10/H12), 3.59 (q, 2H, $^3J_{HH}$ = 7.2, H9/H11, 4.13 (q, 2H, $^3J_{HH}$ = 7.0, H9/H11), 7.46 (m, 2H, H3, H5), 7.57 (t, 1H, $^3J_{HH}$ = 7.4,

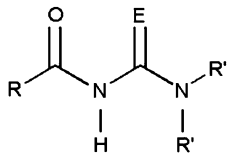

Fig. 1 Structure of the *N*,*N*-dialkyl-*N*′-acyl(aroyl)thio(seleno)urea ligands where R = alkyl or aryl, *R*′ = alkyl. E = S (HL^1), Se (HL^2).

H4), 7.83 (d, 2H, $^3J_{HH}$ = 7.6, H2, H6), 8.59 (br s, 1H, N–H). δ_C (150 MHz; $CDCl_3$): 11.7, 12.8 (C10, C12), 48.4, 51.2 (C9, C11), 127.8 (C3, C5), 128.8 (C2, C6), 132.6 (C1), 132.9 (C4), 162.2 (C7), 180.4 (C8), $^1J(^{13}C–^{77}Se)$ = 220.3.

Bis(*N*,*N*-diethyl-*N*′-benzoylthioureato)cadmium(II). Yield (92.7%); mp 158.0–159.5 °C. Found: C, 49.3, H, 5.1, N, 9.5, S, 10.8. $C_{24}H_{30}N_4O_2S_2Cd$ requires C, 49.4, H, 5.2, N, 9.7, S, 11.0%. δ_H (400 MHz; $CDCl_3$): 1.17 (t, 6H, $^3J_{HH}$ = 7.1, H10/H12), 1.26 (t, 6H, $^3J_{HH}$ = 7.1, H10/H12), 3.70 (q, 4H, $^3J_{HH}$ = 7.1, H9/H11), 3.84 (q, 4H, $^3J_{HH}$ = 7.1, H9/H11), 7.29 (m, 4H, H3, H5), 7.39 (t, 2H, $^3J_{HH}$ = 7.4, H4), 8.03 (d, 4H, $^3J_{HH}$ = 7.1 Hz, H2, H6). δ_C (100 MHz; $CDCl_3$): 12.9, 13.0 (C10, C12), 45.7, 46.1 (C9, C11), 127.5 (C3, C5), 129.4 (C2, C6), 130.8 (C4), 138.1 (C1), 170.9 (C8), 176.6 (C7).

Bis(*N*,*N*-diethyl-*N*′-benzoylselenoureato)cadmium(II). Yield (78.5%); mp 160.1–161.5 °C. Found: C, 42.7; H. 4.4; N, 8.2. $C_{24}H_{30}N_4O_2Se_2Cd$ requires C, 42.6; H, 4.4; N, 8.3%. δ_H (400 MHz; $CDCl_3$): 1.24 (t, 6H, $^3J_{HH}$ = 7.1, H10/H12), 1.35 (t, 6H, $^3J_{HH}$ = 7.1, H10/H12), 3.78 (q, 4H, $^3J_{HH}$ = 7.1, H9/H11), 3.98 (q, 4H, $^3J_{HH}$ = 7.1, H9/H11), 7.33 (m, 4H, H3, H5), 7.44 (t, 2H, $^3J_{HH}$ = 7.3, $^4J_{HH}$ = 2.0, H4), 8.07 (d, 4H, $^3J_{HH}$ = 7.8, H2, H6). δ_C (100 MHz, $CDCl_3$): 13.0, 13.5 (10, C12), 45.8, 48.0 (C9, C11), 127.6 (C3, C5), 129.5 (C2, C6), 131.1 (C4), 137.9 (C1), 167.8 (C8), 170.9 (C7), $^1J(^{13}C–^{77}Se)$ = 164.9.

Synthesis of CdS and CdSe nanoparticles

A typical synthesis was as follows. A specified mass of the precursor complex was dissolved in TOP and injected into a three-neck flask containing HDA at the specified temperature, under a flow of nitrogen. Samples were withdrawn at various time intervals. Following a 60 min reaction period the solution was cooled to 70 °C and excess methanol added to precipitate the nanoparticles. These were isolated by centrifugation and redispersed in toluene to enable further characterisation. No size selective precipitation was performed.

Synthesis of CdSe nanoparticles. The precursor (0.58 g) was suspended in TOP (4 ml) and injected into HDA (5 g) and reacted for 60 min. An initial temperature of 200 °C was used; subsequent identical thermolysis experiments were carried out separately at 100, 125, 150 and 250 °C.

Synthesis of CdS nanoparticles. The precursor (0.5 g) was suspended in TOP (4 ml) and injected into HDA (5 g) and reacted for 60 min. An initial temperature of 200 °C was used; subsequent identical thermolysis experiments were carried out separately at 125, 150 and 240 °C.

Varying precursor concentration for CdS nanoparticles. The precursor (1.25 g) was suspended in TOP (4 ml) and injected into HDA (6 g) at 150 °C followed by a 60 min reaction period.

General experimental

^1H and ^{13}C NMR spectra were recorded on either a 400 MHz Varian^{Unity} Inova spectrometer equipped with an Oxford magnet (9.4 T) operating at 400 MHz for ^1H and 100 MHz for ^{13}C or a 600 MHz Varian^{Unity} Inova spectrometer equipped with an Oxford magnet (14.09 T) operating at 600 MHz for ^1H and 150 MHz for ^{13}C. All samples were measured in deuterated chloroform at concentrations in the order of 10^{-2} M. Proton chemical shifts are quoted relative to the residual $CHCl_3$ solvent resonance at 7.26 ppm, and ^{13}C chemical shifts relative to the $CDCl_3$ triplet at 77.0 ppm (centre peak). *J* values are given in Hz. Elemental analyses were performed on a Heraeus Universal Combustion Analyser, Model CHN-Micro. UV-Vis absorption spectra were obtained using an Agilent 8453 spectrometer and quartz cuvettes (1 cm path length) were used. Samples were determined in toluene which was also used as a reference solvent. Emission spectra were obtained using a Perkin Elmer LS50B Luminescence Spectrometer where the excitation and emission slit widths were set to 5 and 10 nm, respectively. An excitation wavelength of 350 nm was used. X-Ray powder diffraction (XRD) patterns were recorded on an Oxford Xcalibur 2 diffractometer using Mo-Kα radiation (λ = 0.71073 Å) at a temperature of 100 K and with X-ray power = 2.0 kW. Thermogravimetric analyses (TGA) of the precursor compounds were performed using a TG Instruments Q500 thermogravimetric analyser where the samples were maintained in a nitrogen atmosphere and heated at a rate of 10 °C min^{-1}. Transmission electron microscopy (TEM) was performed on either a JEM 1200 EXII (Jeol, Japan) instrument or a LEO 912 Omega (Zeiss, Oberkochen) instrument, fitted with a 2k × 2k digital camera. Samples were prepared by placing a drop of the dilute toluene solution of the sample onto a carbon coated copper grid at room temperature. Excess sample was wicked away using filter paper.

Crystallography

Data collection for the single-crystal determination for *N*,*N*-diethyl-*N*′-benzoylselenourea was performed on a SMART APEX CCD (Bruker-Nonius). Cell refinement and data reduction was performed using SAINT (Bruker-Nonius). Initial structure solution was performed using SHELXS 97 [20] and atomic positions were located from a difference fourier map. The refinement method was full matrix least squares on F^2 using SHELXL 97. Molecular graphics were generated *via* X-Seed[21] using POV-Ray. All hydrogen atoms were placed in geometrically calculated positions with C–H = 0.99 Å, (for $–CH_2$); 0.98 Å, (for $–CH_3$); 0.95 Å, (for phenyl) and refined using a riding model with $U_{iso}(H)$ = 1.2 U_{eq} (parent), for $–CH_2$ and phenyl or $U_{iso}(H)$ = 1.5 U_{eq} (parent) for $–CH_3$.

Crystallographic data are presented in Table 1.

CCDC reference number 622749.

For crystallographic data in CIF or other electronic format see DOI: 10.1039/b618254b

Table 1 Crystal data for *N*,*N*-diethyl-*N*′-benzoylselenourea

Compound	HL^2
Empirical formula	$C_{12}H_{16}N_2OSe$
Formula weight/g mol^{-1}	283.2314
Crystal system	Monoclinic
Space group	*C*2/*c*
a/Å	20.562(4)
b/Å	8.442(2)
c/Å	14.824(3)
β/°	106.93(3)
V/Å^3	2461.7(9)
Z	8
D_c/g cm^{-3}	1.528
F(000)	1152
Temperature/K	173(2)
Absorption coefficient/mm^{-1}	3.032
θ Range for data collection/°	2.07–28.24
Limiting indices, *hkl*	−26 to 26; −11 to 9; −19 to 18
Reflections collected/unique	7430/2851
Radiation	Mo-Kα, graphite monochromated
Refinement method	Full-matrix-least-squares on F^2
Data/restraints/parameters	2851/0/148
Goodness-of-fit on F^2	1.095
Final *R* indices [$I > 2\sigma(I)$]	0.228, 0.0585
R Indices (all data)	$R = 0.0247$, $wR_2 = 0.0592$

Results and discussion

Structural characterisation of *N*,*N*-diethyl-*N*′-benzoylselenourea, (HL^2)

Despite several structural characterisations of metal complexes of *N*,*N*-diethyl-*N*′-benzoylselenourea being available in the literature,[15,22–24] no structural characterisation of the ligand could be found. Fig. 2 shows the molecular structure of HL^2 and Table 2 gives the relevant bond lengths for the compound as well as those of the sulfur analogue.[25]

Table 2 shows that the N–C(O), N–C(E) and (E)C–NR_2 bonds are all shorter than the average C–N single bond length of 1.472(5) Å, consistent with the observed trend for the *N*,*N*-dialkyl-*N*′-aroylthioureas, for which the C–N bond lengths decrease in the order N–C(S) > N–C(O) > S(C)–N.[26] It is noteworthy that the corresponding bond lengths N–C(O) and N–C(E) for HL^1 (E = S) and HL^2 (E = Se), respectively, differ significantly, the N–C(O) for HL^1 being shorter than for HL^2, while the opposite is observed for the N–C(E) bond. This suggests a differing degree of double bond character in these bonds in HL^1 compared to HL^2. In the sulfur analogue HL^1

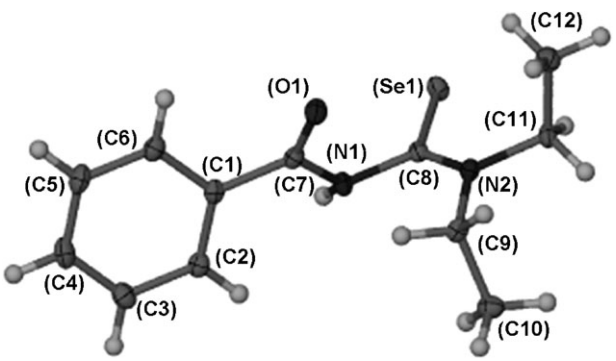

Fig. 2 Molecular structure of *N*,*N*-diethyl-*N*′-benzoylselenourea (HL^2). Displacement ellipsoids are drawn at the 50% probability level.

Table 2 Relevant bond lengths (Å) of HL^1 and HL^2

Bond length	HL^1,[25] E = S	HL^2 E = Se
C═O	1.230(3)	1.221(2)
N–C(O)	1.362(4)	1.388(2)
N–C(E)	1.448(4)	1.416(2)
C═E	1.672(3)	1.834(2)
(E)C–NR_2	1.320(4)	1.320(2)

an intermolecular hydrogen bond between the oxygen atom of the carbonyl group and the thioamidic proton of the neighbouring molecule (symmetry operator; *x*, 1 + *y*, *z*) N(H)···O = 2.012 Å and N–O = 2.871(3) Å, is present,[25] which however is not observed in the selenium analogue. In the case of HL^2, the selenoamidic proton is involved in a weak hydrogen bond with the selenium atom of a neighbouring molecule (symmetry operator 1 − *x*, 1 − *y*, −*z*) N(H)···Se = 2.70 Å and N–Se = 3.532 (2) Å, and the selenoamidic proton of this molecule in turn forms a weak hydrogen bond with the selenium atom of the original molecule, so resulting in a weakly hydrogen bonded dimer in the crystal structure. In terms of hydrogen bonding, the acylselenourea moiety consists of a donor–acceptor pair connected by a delocalized π-system reflected in the shorter amide and acyl-substituted C–N bonds. The formation of a dimer in the crystal lattice by HL^2 therefore represents an example of resonance-assisted hydrogen bonding (RAHB) or π-bond cooperativity.[27] In structures of related acylthiourea ligands, $C_{14}H_9C(O)NHC(S)N(C_2H_5)_2$ and $C_{16}H_9(CH_2)_3C(O)NHC(S)N(C_2H_5)_2$ we have observed a similar RAHB effect,[28] although it is interesting that HL^1 exhibits different hydrogen bonding in the crystal lattice to its selenium counterpart. The relative orientations of the S and O atoms in HL^1 and the Se and O atoms in HL^2 can be defined using the following torsion angles: O–C(O)–N(H)–C(S) = −12.5(4)° and C(O)–N(H)–C(S)–S = −100.4(3)° for HL^1 and O–C(O)–N(H)–C(Se) = 6.9(2) and 108.5(1)° for HL^2. These values show that the coordinating atoms have similar orientations in both HL^1 and HL^2 (Table 2).

NMR spectroscopy

Assignment of the proton and carbon resonances of both the ligands and metal complexes is relatively straightforward, although an interesting aspect of HL^2 and its Cd complex is the presence of the NMR active ^{77}Se nucleus, which couples to the selenocarbonyl carbon atom giving rise to clear satellites, enabling the unambiguous assignment of the selenocarbonyl resonances. As shown in Fig. 3 there are relatively larger differences between the chemical shifts of the C(Se) and C(O) peaks in the ligand compared to the cadmium complex. The C(Se) resonance of HL^2 is more downfield (180.4 ppm) relative to the C(O) resonance (162.2 ppm). In the cadmium complex, the relative chemical shifts are exchanged and the C(Se) resonance is more upfield (167.8 ppm) relative to the C(O) resonance (170.9 ppm). This is probably due to increased electron density and changes in the electronic delocalisation in the chelate ring following loss of H^+ upon coordination to the metal centre. The lower $^1J(^{13}C–^{77}Se)$ coupling of 164.9 Hz in the cadmium complex relative to 220.3 Hz observed in the unbound ligand, also reflects this. Similar observations have

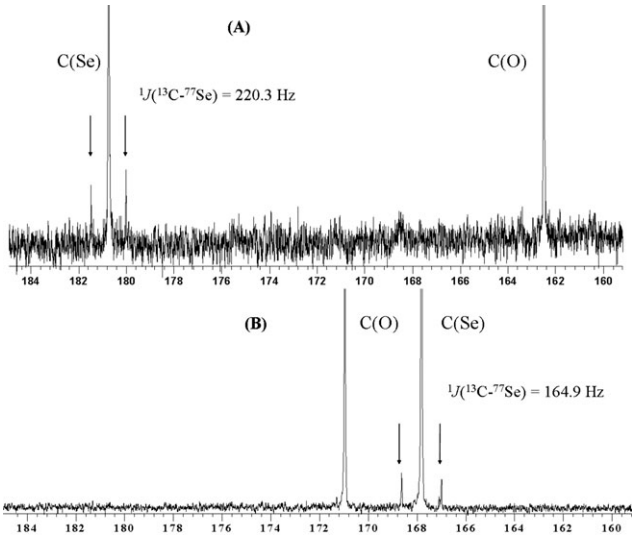

Fig. 3 Expansions of ^{13}C NMR spectra of $C_6H_5CONCSeNC_2H_5$ (A) and $Cd(C_6H_5CONCSeNC_2H_5)_2$ (B), showing $^1J(^{13}C–^{77}Se)$ coupling satellites.

been made for *N*,*N*-dialkyl-*N*′-benzoylthioureas in which ^{13}C enrichment was used to assign the thiocarbonyl and carbonyl carbons resonances unambiguously.[29,30]

Nanoparticle synthesis

Cadmium complexes of *N*,*N*-dialkyl-*N*′-benzoylthio(seleno)-ureas HL^1 and HL^2 readily result in CdS or CdSe nanoparticles on controlled thermolysis. Initially the bis[*N*,*N*-diethyl-*N*′-(benzoylthioureato)]cadmium(II) precursor was thermolysed in TOP and HDA at an injection temperature of 200 °C, to establish whether previously well characterised CdS nanoparticles could be formed. This was found to be the case.

The band edge of 494 nm for the CdS particles formed (Fig. 4) was calculated using the linear regression method and was significantly blue shifted relative to that of bulk CdS (515 nm), indicating quantum confinement.[31] Close to band edge luminescence was observed from the photoluminescence (PL) spectrum and the full width at half maximum height (FWHM) was calculated to be 31.5 nm indicating a relatively narrow particle size distribution. This was confirmed by a

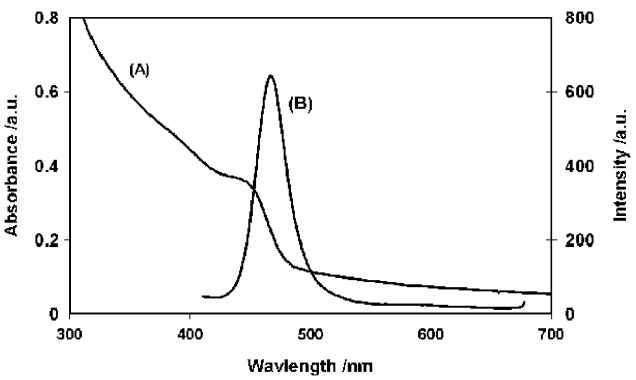

Fig. 4 Optical spectra of CdS nanoparticles: (A) absorption spectrum and (B) photoluminescence spectrum (200 °C, 60 min).

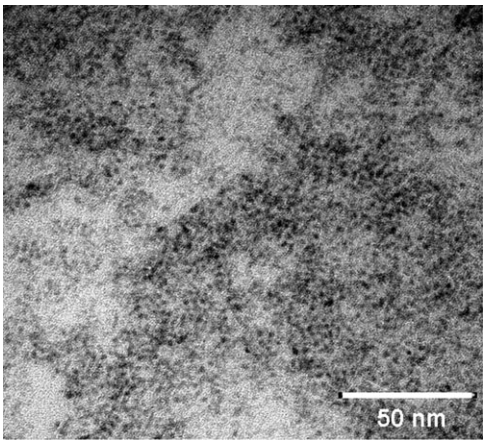

Fig. 5 TEM image of CdS nanoparticles (200 °C, 60 min).

relative standard deviation in the particle size distribution obtained using the TEM image of only 15%.

Spherical nanoparticles of CdS could clearly be seen in the TEM image (Fig. 5) and the average particle size calculated from the TEM data is given in Table 3 as well as data from the optical spectra.

The corresponding selenium analogue, $Cd(C_6H_5CONCSeNC_2H_5)_2$, was thermolysed under similar conditions to those of the sulfur derivative. Well formed, monodispersed spherical nanoparticles of CdSe with an average size of 3.3 (14%) nm were obtained as clearly seen in the TEM image (Fig. 6).

A band edge of 639 nm for the CdSe was obtained from the UV spectrum, this being significantly blue shifted relative to that of bulk CdSe at 716 nm.[7] The PL spectrum (Fig. 7) showed close to band edge luminescence, with the FWHM being slightly larger than in the case of the sulfur analogue at 51 nm. This indicates a larger particle size distribution although this is not reflected in the standard deviation obtained from the TEM image.

It is well known that both bulk CdS and CdSe have stable wurtzite phases at room temperature,[32] however both types of crystallites can exist in either the cubic or hexagonal phases. The small particle size of both the CdS and CdSe nanoparticles however complicates the assignment of a specific phase and it becomes difficult to exclusively assign a particular phase to each sample. Bawendi *et al*. have also reported that a mixture of the two phases is possible for CdSe nanoparticles where one phase can dominate the other.[33] The X-ray diffraction patterns of the CdS and CdSe nanoparticles synthesised here (Fig. 8 and 9) are interestingly consistent with a predominantly cubic phase in both cases, although this phase is not necessarily exclusive.

The broad peaks in both the CdS and CdSe diffraction patterns are indicative of particles in the nanosize domain and the (111), (220) and (311) planes of cubic CdS and CdSe are clearly visible.

Effects of variation of thermolysis conditions

Recent reports in the literature have shown that variations in reaction temperature can significantly affect the morphology of the resulting nanoparticles.[34,35] We examined the role of

Table 3 Properties of CdS and CdSe nanoparticles obtained at various temperatures from thermolysis of bis[*N*,*N*-diethyl-*N*′-(benzoylselenoureato)]cadmium(II) and bis[*N*,*N*-diethyl-*N*′-(benzoylthioureato)]cadmium(II)

	Temp./°C	Band edge/nm	Band edge/eV	Average size[a]/nm (std. dev. %)	Average size/nm (Scherrer equation[36])	Emission maxima/nm
CdSe	100	515	2.41	2.0 (14)	—	504 453[b]
	125	539	2.30	2.2 (13)	1.3	522.5 451.5[b]
	150	575	2.15	2.5 (15)	1.7	557.5
	200	639	1.94	3.3 (14)	1.6	589.5
	250	688	1.80	3.8 (15)	1.7	611
CdS	125	480	2.58	3.1 (18)	—	441.5 516.5[b]
	150	464	2.67	3.0 (15)	1.6	452.5
	200	494	2.51	3.5 (15)	1.9	467.0
	240	562	2.21	3.9 (13)	—	474.0

[a] From TEM data. [b] Second, smaller maximum.

temperature on the thermolysis of bis[*N*,*N*-diethyl-*N*′-(benzoylselenoureato)]cadmium(II) and bis[*N*,*N*-diethyl-*N*′-(benzoylthioureato)]cadmium(II), results of which are shown in Table 3.

For bis[*N*,*N*-diethyl-*N*′-(benzoylselenoureato)]cadmium(II), it is remarkable that CdSe nanoparticle formation occurred at a temperature as low as 100 °C. Samples withdrawn from the reaction vessel at varying times resulted in particles for which the band edge (502 nm) and the emission maximum (487 nm) at this temperature was only marginally red shifted over time. A second smaller emission maximum appeared however at 453 nm, the intensity of which increased with time. This phenomenon was also observed at 125 °C at which temperature the band edge red shifted only marginally over time as did the emission maxima; however the smaller emission maximum at 453 nm persisted and grew in intensity as the reaction progressed. Nevertheless the overall intensity of the latter minor emission band decreased with increasing temperature (21.5% of the emission maxima at 100 °C to 8.2% of the emission maxima at 125 °C and was no longer observable at temperatures >150 °C). At temperatures >150 °C good quality nanoparticles with comparable optical spectra were obtained. Surprisingly quantum confinement still occurred at 250 °C since the band edge of 699 nm remained blue shifted relative to that of bulk CdSe although (at 250 °C) the emission broadened significantly over time suggesting the formation of a polydisperse distribution of CdSe particle sizes.

Particle sizes estimated from the TEM images as well as the (220) peak in the XRD data[36] are shown in Table 3. The reduced crystallinity of the particles obtained at 100 °C precluded particle size estimation and no data is shown. Particle sizes calculated using the Scherrer equation[36] are consistently smaller than those obtained from the TEM images, although the trend of increasing particle size with increasing temperature is consistent with TEM observation. It is noteworthy that the particle morphology remained similar throughout the temperature study; essentially only spherical particles were obtained.

Examining data obtained for CdS nanoparticle formation shows that at an injection temperature of 125 °C, relatively poor quality CdS nanoparticles were obtained. It is likely that at this relatively low decomposition temperature slow nucleation occurs, and this is supported by the yellow colour due to nucleation in the solution only being observed 12 min into the reaction, whereas at higher temperatures (200 °C) this yellow colour is immediately observable. The uneven nucleation results in a broad particle size distribution reflected in the higher standard deviation of 18% and the bimodal emission evident in the PL spectrum. An injection temperature of

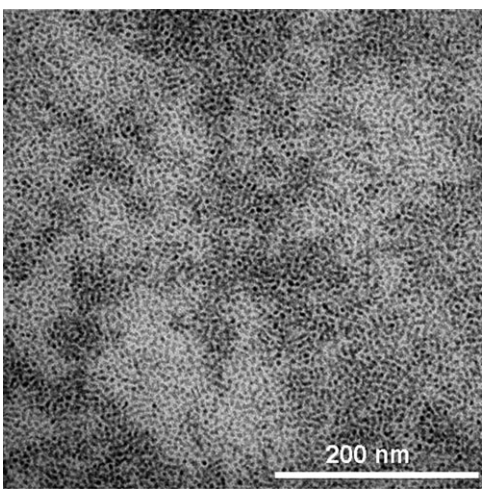

Fig. 6 TEM image of CdSe nanoparticles (200 °C, 60 min).

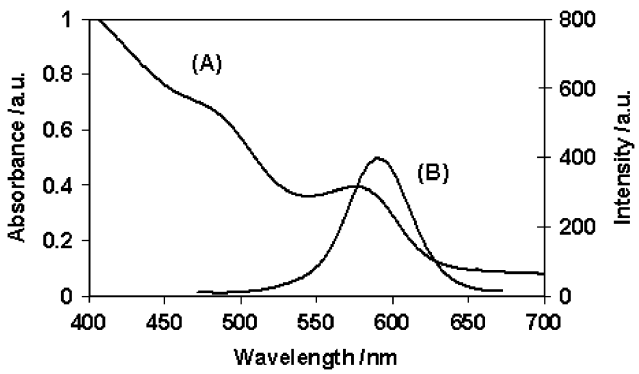

Fig. 7 Optical spectra of CdSe nanoparticles: (A) absorption spectrum and (B) photoluminescence spectrum (200 °C, 60 min).

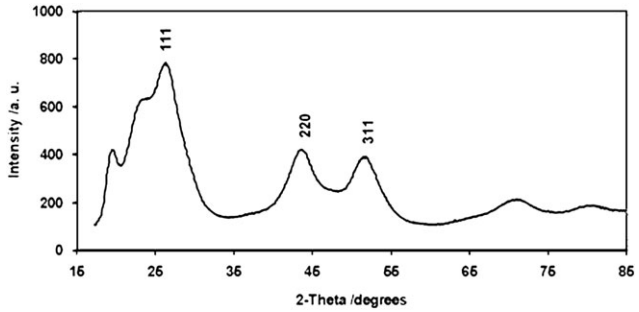

Fig. 8 X-Ray diffraction pattern of CdS nanoparticles (200 °C, 60 min).

150 °C resulted in nanoparticles with the smallest diameter and a band gap of 464 nm. This is significantly blue shifted relative to that of bulk CdS at 515 nm indicating quantum confinement. The absorption spectrum obtained from a sample withdrawn 10 min into the reaction at 150 °C, was very similar to that from the 60 min sample indicating that nucleation occurs more rapidly at a higher temperature. The PL spectrum obtained from the same 10 min sample, showed an emission maximum at 447 nm, but with clear evidence of longer wavelength emission. As the reaction time increased this emission was significantly reduced and is barely observable in the spectrum obtained at 60 min. This indicates that annealing and passivation of the semiconducting surface occurs as the reaction proceeds. At an even higher injection temperature of 240 °C, the reaction becomes uncontrollable as within 20 min the particles are no longer in the region of quantum confinement. In contrast the formation of relatively good quality CdSe nanoparticles starts at relatively lower temperatures (100 °C) but results in particles with a relatively narrow size distribution over the entire temperature range, the CdSe particles retaining quantum confinement up to 250 °C.

Particle sizes estimated from the (220) peak in the XRD data using the Scherrer equation are given in Table 3.[36] CdS particle sizes for the 125 and 240 °C samples are not given due to the reduced crystallinity observed in these samples. It is interesting to note that whilst the average diameter of the nanoparticles did vary with the injection temperature, the final morphology of the particles remained unaltered for both CdS and CdSe obtained in this manner.

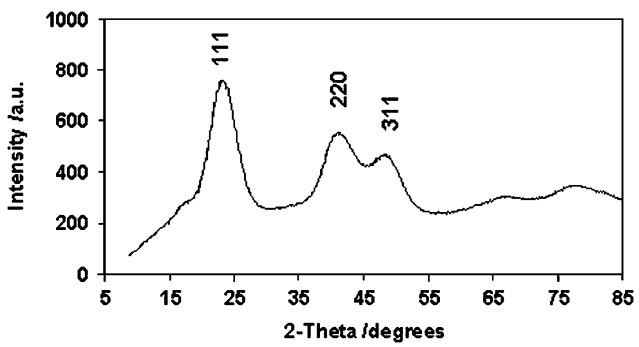

Fig. 9 X-Ray diffraction pattern of CdSe nanoparticles (200 °C, 60 min).

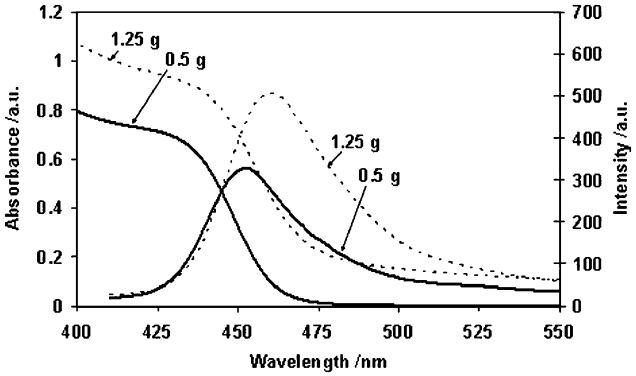

Fig. 10 Optical spectra of CdS at varying precursor concentrations: (A) absorption and (B) photoluminescence spectra (200 °C, 60 min).

The effect of precursor complex concentration was investigated using bis[*N*,*N*-diethyl-*N*′-(benzoylthioureato)]cadmium(II) where a 2.5-fold increase in the precursor concentration (0.5–1.25 g of precursor) led to the optical spectra shown in Fig. 10. A red shift in the band edge and a broader emission indicate larger and more polydisperse nanoparticles, however, the morphology of the particles remained constant with increased precursor concentration.

The thermogravimetric (TGA) decomposition data for both bis[*N*,*N*-diethyl-*N*′-(benzoylselenoureato)]cadmium(II) and bis[*N*,*N*-diethyl-*N*′-(benzoylthioureato)]cadmium(II) is shown in Fig. 11. Thermal decomposition of *N*,*N*-dialkyl-*N*′-benzoylselenourea metal complexes have not been reported, although there are reports on the thermal decomposition of the related *N*,*N*-dipropyl- and dihexyl-*N*′-(benzoylthioureato)cadmium(II) complexes indicating that the mass loss and residue formed correspond to the formation of cadmium sulfide.[37] Our data is consistent with these findings, as shown in Table 4 for the formation of CdS as well as CdSe.

Assuming that the mass loss during thermal decomposition is a first-order process, a Coats–Redfern analysis[38] can be performed to estimate the activation energy of our precursors resulting in cubic phases of either CdSe or CdS. This analysis gave activation energies in the range of 18–23 kJ mol^{-1} for the selenourea complex Cd($C_6H_5CONCSeNC_2H_5$)$_2$, and 28–39 kJ mol^{-1} for the thiourea complex, Cd($C_6H_5CONCSNC_2H_5$)$_2$. Activation energies between 10.9 and 18.2 kJ mol^{-1} for

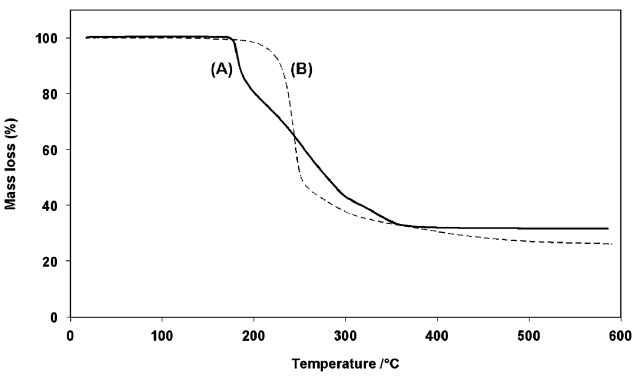

Fig. 11 Thermal decomposition of Cd($C_6H_5CONCSeNC_2H_5$)$_2$ (A) and Cd($C_6H_5CONCSNC_2H_5$)$_2$ (B) precursors.

Table 4 TGA results of precursors

Precursor	Temp. range/°C	Found mass (%)	Calc. mass for CdE (%)
$Cd(C_6H_5CONCSeNC_2H_5)_2$	175–377	31.0	28.3
$Cd(C_6H_5CONCSNC_2H_5)_2$	200–501	25.8	24.8

several, related single-source precursors, resulting in the formation of only *spherical* nanoparticles have recently been published.[39] In this context, Nair and Scholes recently suggested that single compound precursors with much lower activation energies, in the region of 2.1 kJ mol^{-1}, were shown to result in particles showing anisotropic growth as a result of *kinetically controlled growth*, giving rise to CdS nanorods, rather than spherical CdS particles, resulting from more thermodynamically stable precursors such as ours. It should be emphasized here that the non-spherical particles obtained were hexagonally phased, whereas those described in this paper form in a cubic phase, so that any inference from these finding should be made with caution.

Conclusions

In conclusion the conveniently prepared bis[*N*,*N*-diethyl-*N*′-(benzoylthioureato)]cadmium(II) and its corresponding selenourea analogue, bis[*N*,*N*-diethyl-*N*′-(benzoylselenoureato)]cadmium(II), may be used as single-source precursors for the synthesis of HDA stabilised, spherical CdS and CdSe nanoparticles, respectively, which show quantum confinement. From the XRD data it is clear that both CdS and CdSe particles are readily formed from these precursors which are predominantly in the cubic phase. Thermolysis of bis[*N*,*N*-diethyl-*N*′-(benzoylthioureato)]cadmium(II) and, the somewhat thermodynamically less stable bis[*N*,*N*-diethyl-*N*′-(benzoylselenoureato)]cadmium(II), over a range of increasing temperatures (100–200 °C) shows that essentially only spherical CdS and CdSe nanoparticles were obtained, independent of the reaction temperature and the precursor concentration employed. This suggests thermodynamic growth control of CdS and CdSe from these precursors, respectively.

Acknowledgements

Financial support from the University of Stellenbosch, the NRF, (GUN 2046827), THRIP (project 2921) and Anglo-platinum Ltd, is gratefully acknowledged. J. B. acknowledges a Harry Crossley bursary.

References

1 M. A. Malik, N. Revaprasadu and P. O'Brien, *Chem. Mater.*, 2001, **13**, 913–920.
2 M. C. Schlamp, X. Peng and A. P. Alivisatos, *J. Appl. Phys.*, 1997, **82**, 5837–5842.
3 W. C. W. Chan and S. Nie, *Science (Washington, D. C.)*, 1998, **281**, 2016–2018.
4 V. I. Klimov, A. A. Mikhailovsky, S. Xu, A. Malko, J. A. Hollingsworth, C. A. Leatherdale, H. J. Eisler and M. G. Bawendiz, *Science (Washington, D. C.)*, 2000, **290**, 314–317.
5 S. Coe, W.-K. Woo, M. Bawendi and V. Bulovic, *Nature (London)*, 2002, **420**, 800–803.
6 W. U. Huynh, J. J. Dittmer and A. P. Alivisatos, *Science (Washington, D.C.)*, 2002, **295**, 2425–2427.
7 C. B. Murray, D. J. Norris and M. G. Bawendi, *J. Am. Chem. Soc.*, 1993, **115**, 8706–8715.
8 M. Azad Malik, P. O'Brien and N. Revaprasadu, *J. Mater. Chem.*, 2001, **11**, 2382–2386.
9 Y.-w. Jun, S.-M. Lee, N.-J. Kang and J. Cheon, *J. Am. Chem. Soc.*, 2001, **123**, 5150–5151.
10 P. S. Nair, T. Radhakrishnan, N. Revaprasadu, G. Kolawole and P. O'Brien, *J. Mater. Chem.*, 2002, **12**, 2722–2725.
11 P. S. Nair, T. Radhakrishnan, N. Revaprasadu, G. A. Kolawole and P. O'Brien, *Chem. Commun.*, 2002, 564–565.
12 P. Sreekumari Nair, T. Radhakrishnan, N. Revaprasadu, G. A. Kolawole and P. O'Brien, *Polyhedron*, 2003, **22**, 3129–3135.
13 M. J. Moloto, N. Revaprasadu, P. O'Brien and M. A. Malik, *J. Mater. Sci.: Mater. Electron.*, 2004, **15**, 313–316.
14 M. Merdivan, N. Kulcu and S. Aygun, *Kim. Kim. Muhendisligi Semp, 8th*, 1992, **1**, 31–34.
15 W. Bensch and M. Schuster, *Z. Anorg. Allg. Chem.*, 1993, **619**, 791–795.
16 L. Beyer, E. Hoyer, H. Hennig, R. Kirmse, H. Hartmann and J. Liebscher, *J. Prakt. Chem.*, 1975, **317**, 829–839.
17 M. Schuster and K. H. Koenig, *Fresenius' Z. Anal. Chem.*, 1988, **331**, 383–386.
18 I. B. Douglass, *J. Am. Chem. Soc.*, 1937, **59**, 740–742.
19 I. B. Douglass and F. B. Dains, *J. Am. Chem. Soc.*, 1934, **56**, 1408–1409.
20 G. M. Sheldrick, *Suite of programs for crystal structure determination and refinement*, University of Gottingen, Germany, 1997.
21 L. J. Barbour, *J. Supramol. Chem.*, 2003, **1**, 189.
22 W. Bensch and M. Schuster, *Z. Anorg. Allg. Chem.*, 1993, **619**, 786–790.
23 W. Bensch and M. Schuster, *Z. Anorg. Allg. Chem.*, 1994, **620**, 1479–1482.
24 W. Bensch and M. Schuster, *Z. Anorg. Allg. Chem.*, 1994, **620**, 177–182.
25 M. Bolte and L. Fink, personal communication to CCDC, 2003 (CCDC 214315).
26 K. R. Koch, C. Sacht, T. Grimmbacher and S. Bourne, *S. Afr. J. Chem.*, 1995, **48**, 71–77.
27 T. Steiner, *Angew. Chem., Int. Ed.*, 2002, **41**, 48–76.
28 J. C. Bruce and K. R. Koch, unpublished results, 2004.
29 K. R. Koch and M. C. Matoetoe, *Magn. Reson. Chem.*, 1991, **29**, 1158–1160.
30 A. N. Mautjana, J. D. S. Miller, A. Gie, S. A. Bourne and K. R. Koch, *Dalton Trans.*, 2003, 1952–1960.
31 T. Trindade, P. O'Brien and N. L. Pickett, *Chem. Mater.*, 2001, **13**, 3843–3858.
32 R. J. Bandaranayake, G. W. Wen, J. Y. Lin, H. X. Jiang and C. M. Sorensen, *Appl. Phys. Lett.*, 1995, **67**, 831–833.
33 M. G. Bawendi, A. R. Kortan, M. L. Steigerwald and L. E. Brus, *J. Chem. Phys.*, 1989, **91**, 7282–7290.
34 Y. Li, X. Li, C. Yang and Y. Li, *J. Mater. Chem.*, 2003, **13**, 2641–2648.
35 A. A. Memon, M. Afzaal, M. A. Malik, C. Q. Nguyen, P. O'Brien and J. Raftery, *Dalton Trans.*, 2006, 4499–4505.
36 B. D. Cullity, *Elements of X-ray Diffraction*, Addison–Wesley Publishing Company, New York, 2nd edn, 1978.
37 M. Merdivan, F. Karipcin, N. Kulcu and R. S. Aygun, *J. Therm. Anal. Calorim.*, 1999, **58**, 551–557.
38 A. W. Coats and J. P. Redfern, *Nature (London)*, 1964, **201**, 68–69.
39 P. S. Nair and G. D. Scholes, *J. Mater. Chem.*, 2006, **16**, 467–473.